



HAL
open science

Gum Arabic and chitosan self-assembly: Thermodynamic and mechanism aspects

Marie E. Vuillemin, Florentin Michaux, Lionel Muniglia, Michel Linder,
Jordane Jasniewski

► To cite this version:

Marie E. Vuillemin, Florentin Michaux, Lionel Muniglia, Michel Linder, Jordane Jasniewski. Gum Arabic and chitosan self-assembly: Thermodynamic and mechanism aspects. Food Hydrocolloids, 2019, 10.1016/j.foodhyd.2019.05.048 . hal-02146529

HAL Id: hal-02146529

<https://hal.science/hal-02146529>

Submitted on 25 Oct 2021

HAL is a multi-disciplinary open access archive for the deposit and dissemination of scientific research documents, whether they are published or not. The documents may come from teaching and research institutions in France or abroad, or from public or private research centers.

L'archive ouverte pluridisciplinaire **HAL**, est destinée au dépôt et à la diffusion de documents scientifiques de niveau recherche, publiés ou non, émanant des établissements d'enseignement et de recherche français ou étrangers, des laboratoires publics ou privés.



Distributed under a Creative Commons Attribution - NonCommercial 4.0 International License

1 **Gum Arabic and chitosan self-assembly: thermodynamic and mechanism**
2 **aspects**
3

4 Marie E. Vuillemin, Florentin Michaux, Lionel Muniglia, Michel Linder and Jordane

5 Jasniewski *

6 *Corresponding author: jordane.jasniewski@univ-lorraine.fr

7 Université de Lorraine, LIBio, F-54000 Nancy, France

8 **Abstract**

9 The interactions between gum Arabic (GA) and chitosan (CN) in solution have been
10 investigated upon pH (4.5, 5.0 and 5.5) and temperature (5, 25 and 45 °C). Isothermal titration
11 calorimetry (ITC) has been used to determine the thermodynamic parameters involved in the
12 complex coacervation process between these two polymers. Zeta potential, turbidity
13 measurements and optical microscopy were used as complementary methods to have a better
14 understanding of the phenomenon at the origin of the self-assembly. Unlike data already
15 published by authors, concerning the GA-CN coacervation model, a raise in temperature
16 seemed to favor electrostatic interactions. The enthalpy became more favorable upon
17 temperature, a phenomenon probably related to the availability of CN charges. A raise in
18 temperature would lead to a compaction of CN, decreasing its steric hindrance during self-
19 assembly. According to all experiments conducted in this study, the GA/CN interaction optimal
20 molar ratio would be 4:1. However, this optimal ratio changed upon pH-temperature
21 combinations. The results presented in this study should lead to a better understanding of the
22 interactions between charged polymers and in the end, help in their application in the food,
23 pharmaceutical and cosmetic industries.

24 **Keywords:** Complex coacervation; interactions; Isothermal titration calorimetry; gum Arabic;
25 chitosan; self-assembly

26 **1. Introduction**

27 Complex coacervation is a phenomenon in which polyelectrolytes interact to form a liquid
28 phase rich in polymer called coacervate and an equilibrium phase poor in polymer called the
29 diluted phase (Kizilay, Kayitmazer, & Dubin, 2011). It is used in the industry to encapsulate
30 several molecules of interest such as vitamins, plants oils and flavors (Bhatia, Khattak, &
31 Roberts, 2005; Lankalapalli & Kolapalli, 2009). This bottom-up approach is a construction of
32 complexes by self-assembly of molecules due to interactions between two polymers, which
33 depend on changes in environmental conditions, such as pH, ionic strength, temperature, or
34 concentration (Joye & McClements, 2014; Kim, Yang, Park, Lim, & Cha, 2017; Schmitt &
35 Turgeon, 2011). This eco-friendly approach does not need an external energy contribution and
36 is performed under soft conditions (in aqueous medium). Several polyelectrolytes are suitable
37 for this approach such as proteins and polysaccharides. Polysaccharides are good candidates for
38 complex coacervation because they can be charged in solution, they are not expensive, readily
39 available, bio-compatible and have low toxicity (Anwunobi & Emeje, 2011). Complex
40 coacervation of polyelectrolytes has been studied by several authors (Kayitmazer, 2017; Priftis,
41 Laugel, & Tirrell, 2012; Veis, 2011) who agreed that different parameters drive the formation
42 of complexes. Early studies (Overbeek & Voorn, 1957) suggested that coacervation results from
43 electrostatic attractions. Most of the time, the two polyelectrolytes attract each other because
44 they are oppositely charged, forming complexes prior to coacervation (Veis & Aranyi, 1960).
45 When the two oppositely-charged polymers form a complex driven by electrostatic interaction,
46 counterions and water molecules are released in the bulk, contributing to an entropy gain of the
47 system.

48 In this study, complex coacervation between chitosan (CN) and gum Arabic (GA), two
49 polysaccharides of opposite charges, has been studied through thermodynamic and mechanistic
50 aspects. CN is a β (1-4)-linked glucosamine which is found in the cellular wall of zygomycetes,
51 bacteria and yeast. The main source of CN comes from the deacetylation under alkaline
52 conditions of the chitin of crustaceans shells. This biopolymer is film-forming, biodegradable
53 and biocompatible. It exhibits antimicrobial and antioxidant activities (Fathi, Martín, &
54 McClements, 2014; Soni, Mahmoud, Chang, El-Giar, & Hassan, 2018; Sonia & Sharma, 2012).
55 Furthermore, CN is well-known for presenting a large density of positive charges (Fathi et al.,
56 2014). In order to have a coacervation phenomenon with CN, GA was chosen as polyanion.
57 This polymer comes from an exudate from the stems and branches of acacia trees, which grow
58 across the Sahelian belt of Africa (*Acacia senegal* and *Acacia seyal*) (Lopez-Torrez, Costalat,
59 Williams, Doco, & Sanchez, 2015). It is an effective encapsulation agent due to its high water
60 solubility, the low viscosity of concentrated solutions and its ability to act as an oil-in-water
61 emulsifier. Furthermore, GA is often used as polyanion in several studies on complex
62 coacervation (Aberkane, Jasniewski, Gaiani, Scher, & Sanchez, 2010; Butstraen & Salaün,
63 2014; Eratte, Wang, Dowling, Barrow, & Adhikari, 2014; Shaddel et al., 2018). GA is
64 essentially made of polysaccharides and salts. It contains three different fractions: 85-90 wt. %
65 of arabinogalactan, 10 wt. % of arabinogalactan-protein complex and 2 wt. % of one or two
66 glycoproteins (Lopez-Torrez et al., 2015). The fractions containing proteins, responsible for the
67 surfactant activity of the GA, are found in higher amount in *Acacia senegal* exudate than in the
68 one of *Acacia seyal* (1.8% w/w vs. 0.9% w/w, respectively) (Lopez-Torrez et al., 2015). In this
69 study, the dialyzed total gum was used. Ionized CN (pKa from 6.3 to 7.0 (Beppu & Santana,
70 2002)) has an extended conformation in acetic acid solution, so its charges are accessible
71 (Espinosa-Andrews, Báez-González, Cruz-Sosa, & Vernon-Carter, 2007; Schatz et al., 2004).
72 Ionized GA (pKa close to 3.6 (Aberkane et al., 2010)) has a globular structure (Moschakis,

73 Murray, & Biliaderis, 2010; Renard, Garnier, Lapp, Schmitt, & Sanchez, 2012) in aqueous
74 solution. The influence of pH, ionic strength, temperature, or polyelectrolytes concentration on
75 GA and CN coacervation has already been studied by several authors (Avadi et al., 2010a,
76 2010b; Butstraen & Salaün, 2014; Espinosa-Andrews et al., 2007; Espinosa-Andrews,
77 Sandoval-Castilla, Vázquez-Torres, Vernon-Carter, & Lobato-Calleros, 2010; Maqbool, Ali, &
78 Alderson, 2010; Roldan-Cruz, Carmona-Ascencio, Vernon-Carter, & Alvarez-Ramirez, 2016;
79 Sakloetsakun, Preechagoon, Bernkop-Schnürch, & Pongjanyakul, 2015; Tan, Xie, Zhang, Cai,
80 & Xia, 2016). However, the comprehension of the coacervates formation mechanism is still an
81 issue to be tackled. This study aimed to better understand this mechanism by determining the
82 corresponding thermodynamic parameters (stoichiometry, entropy and enthalpy) using
83 Isothermal Titration Calorimetry to understand what drove the complex coacervation between
84 these two polymers. Another aim of this work was to understand the part played by the different
85 parameters to shed some light on the mechanism of this phenomenon.

86 **2. Materials and Methods:**

87 **2.1. Materials**

88 Chitosan (CN) MMW (medium molecular weight, Mw 310 kDa, deacetylation degree of 75%)
89 was purchased from Sigma-Aldrich (France). Gum Arabic (GA) Instantgum AA from *Acacia*
90 *senegal* (Mw 400 kDa (Renard, Lavenant-Gourgeon, Ralet, & Sanchez, 2006)) was a gift from
91 Nexira (France). Acetic acid, NaOH and ultrapure water were of analytical grade.

92 **2.2. Methods**

93 **2.2.1. Polymers purification**

94 CN and GA were dialyzed against acetic acid (1% v/v) and water, respectively, with a
95 high grade regenerated membrane (MWCO 10 000 Da from Membrane Filtration Products Inc.)
96 to eliminate excess salts. Dialysis was stopped when the conductivity outside the membrane
97 was equal to the one of acetic acid (1% v/v) or ultrapure water, respectively. Samples were
98 centrifuged then for 30 min at 12 000 g to remove insoluble material and air bubbles and then
99 freeze-dried and stored at 4 °C. **The molecular weights of both polysaccharides were verified**
100 **by SEC-MALLS measurement post-dialysis and were very close to the ones provided by the**
101 **suppliers.**

102 **2.2.2. Polymers stock solutions preparation**

103 CN 0.02% w/v (6.45×10^{-4} mM) and GA 1.00% w/v (2.50×10^{-2} mM) stock solutions were
104 prepared by dissolving purified CN or GA in acetic acid (1% v/v in ultrapure water). The
105 solutions were stirred on a magnetic plate at 400 rpm overnight at 4 °C to make sure the
106 polymers were completely dissolved. Though GA is soluble in water, the mixtures were made
107 by adding GA solubilized in acetic acid, so the dilution of acetic acid in water signal would not
108 interfere with the polymers interaction signal, during ITC measurements when GA solution was
109 added to CN solution. The CN solution was prepared at 0.02% w/v (6.45×10^{-4} mM),
110 concentration for which its viscosity was low enough.

111 **2.2.3. Polymers mixtures preparation**

112 Polymers mixtures were prepared at different temperatures (5, 25 and 45 °C), at different
113 pH (4.5, 5.0 and 5.5 by adding either acetic acid (1 N) or NaOH (5 N) as required), and different

114 polymers molar ratio. After pH adjustment, the required amount of polymer solutions recovered
115 from stocks solutions were placed 15 min in a thermostatic degassing chamber to reach the
116 targeted temperature and remove bubbles. GA solutions were then added to CN solutions and
117 then analyzed after 5 min to compare samples in identical conditions.

118 **2.2.4. Isothermal titration calorimetry (ITC)**

119 ITC measurements were carried out with an Affinity ITC equipped with a standard
120 volume (965 μL) gold cell (TA instruments, Waters SAS, France) to measure the dissociation
121 constant (K_d) and the enthalpic variation due to interaction between CN and GA. The entropy
122 and the Gibbs free energy were obtained from the following equations:

$$123 \quad \Delta G = - R.T.\ln(1/K_d) \quad (\text{Eq. 1})$$

$$124 \quad T\Delta S = \Delta H - \Delta G \quad (\text{Eq. 2})$$

125 With ΔG : Gibbs free energy variation ($\text{kJ}\cdot\text{mol}^{-1}$), ΔH : enthalpy variation ($\text{kJ}\cdot\text{mol}^{-1}$), ΔS :
126 entropy variation ($\text{kJ}\cdot\text{mol}^{-1}\cdot\text{K}^{-1}$), T : temperature (K) and R is the specific gas constant
127 ($8.3144598 \text{ J}\cdot\text{mol}^{-1}\cdot\text{K}^{-1}$).

128 Ultrapure water was used in the reference cell. All solutions were degassed under vacuum
129 for 15 min using the associated degassing station (TA instruments, Waters SAS, France) at the
130 temperature of titration (5, 25 or 45 $^{\circ}\text{C}$). The injector microsyringe (320 μL), was loaded with
131 stock solution of GA (1.00% w/v GA (2.50×10^{-2} mM) in 1.00% v/v acid acetic solution). 5 μL
132 were sequentially injected 50 times each 300 s to the titration cell (volume = 965 μL) filled with
133 CN solution (0.02% w/v CN (6.45×10^{-4} mM) in 1.00% v/v acid acetic solution). The polymers
134 concentrations were chosen based on preliminary measurements to optimize concentrations in
135 order to have complete titrations without signal saturation. For each measurement, the pH, the

136 temperature and the acetic acid solvent were the same in the cell and in the syringe to limit the
137 dilution effect. The heat of dilution from the blank titration was subtracted from the raw data in
138 all experiments. Data acquisition was performed using the ITC Run software and data were
139 analyzed with the NanoAnalyse software (TA instruments, Waters SAS, France). The
140 “Independent” model was chosen as the best model from the plot residual values to fit the
141 obtained isotherms. All measurements were made in triplicate.

142 **2.2.5. Approximate Zeta potential**

143 The approximate Zeta potential of the polymers alone (0.02 w/v for CN (6.45×10^{-4} mM)
144 and 1.00% w/v for GA (2.50×10^{-2} mM)) and of the mixtures were calculated from measurement
145 of the electrophoretic mobility at controlled temperatures (5, 25 and 45 °C) using a Zetasizer
146 Nano-ZS instrument (Malvern Panalytical, United Kingdom) equipped with a He/Ne ion laser
147 ($\lambda = 532$ nm). Measurements were collected on a detector at 173°. An automatic titrator
148 (Malvern Multipurpose Titrator MPT2) was also used for the automation of Zeta potential
149 measurements upon the GA/CN molar ratio (0.02 w/v for CN (6.45×10^{-4} mM) and 1.00% w/v
150 for GA (2.50×10^{-2} mM)). 25 injections of 124 μ L of GA solution were made in 12 mL of CN
151 solution. Investigated solution was filled into a Zeta potential folded capillary cell (DTS1070,
152 Malvern Panalytical). The instrument determined the Zeta potential with the Smoluchowski
153 equation (Jayme, Dunstan, & Gee, 1999). All measurements were made in triplicate.

154 **2.2.6. Turbidity measurements**

155 Turbidities of the GA/CN mixtures were measured with a UV-visible spectrophotometer
156 (Shimadzu 1280, Japan) at 660 nm. The transmittance (T) of the spectrophotometer was
157 calibrated with 0.1 N acetic acid to 100% and the turbidity of the samples was reported as 100-
158 T%. The relative turbidity (τ) was calculated from the equation 3:

159
$$\tau = -\frac{1}{L} \ln \frac{I_t}{I_0} \quad (\text{Eq. 3})$$

160 Where L was the optical path length (1 cm) and I_t and I_0 were the transmitted light
161 intensity and the incident light intensity, respectively. All measurements were made in
162 triplicate.

163 **2.2.7. Optical microscopy**

164 The mixtures were observed by optical microscopy (Olympus BH2, Japan) at x40
165 magnification. The images were recorded with a CMOS 5 MPixel camera (Olympus) under the
166 control of ToupView software. The micrographs presented are representative of the samples.
167 They were analyzed by using an image analysis software (ImageJ) in order to obtain the
168 particles size and number. Polydispersity index of the sample was obtained using equation 4:

169
$$\text{Polydispersity index} = \left(\frac{\text{Standard deviation}}{\text{Average size}} \right)^2 \quad (\text{Eq. 4})$$

170 **2.2.8. Statistical analysis**

171 The values were expressed in mean \pm standard deviation. Differences between mean
172 values were assessed using the one-way analysis of variance (ANOVA) which was performed
173 using Excel for Statistical Analysis and XLSTAT. Differences were considered statistically
174 significant when p_{value} was below 0.05.

175 **3. Results and discussion:**

176 **3.1. pH influence over the approximate Zeta potentials of GA and CN**

177 Complex coacervation depends on a few parameters, such as: polymer ratio, total polymer
178 concentration, polymer backbone flexibility, polymer charges, ionic strength and pH (de Kruif,

179 Weinbreck, & de Vries, 2004; Espinosa-Andrews et al., 2007; Sanchez, Mekhloufi, & Renard,
180 2006; Schmitt, Sanchez, Desobry-Banon, & Hardy, 1998; Turgeon, Schmitt, & Sanchez, 2007).
181 Since coacervation is supposed to be mostly driven by electrostatic interactions, the influence
182 of the pH on the coacervate formation was first investigated. The chosen pH range was 4.5 to
183 5.5. Below pH 3.5, carboxylic groups of GA were protonated and contraction of its molecular
184 backbone could suppress the coacervation phenomenon (Espinosa-Andrews et al., 2007). For
185 pH values above 6.0, close to CN pKa, its degree of ionization and its solubility decreased
186 (Espinosa-Andrews et al., 2007; Sonia & Sharma, 2012).

187 From **Table 1** CN and GA were charged in the chosen pH range. The pH strongly
188 modified the CN surface charge but not the one of GA. The approximate Zeta potential of CN
189 in acetic acid solution was thus higher at pH 4.5 (37.2 ± 3.1 mV) than at pH 5.5 (24.5 ± 1.9
190 mV) at 5 °C and twice higher at 5 °C (37.2 ± 3.1 mV) than at 45 °C (17.8 ± 0.8 mV) at pH 4.5.
191 The CN Zeta potential decreased upon pH and temperature, which was consistent with the
192 literature (Fan, Yan, Xu, & Ni, 2012; Filion, Lavertu, & Buschmann, 2007). GA charge in acetic
193 solution did not change upon pH. The pKa of CN was in a range from 6.3 to 7.0 (Beppu &
194 Santana, 2002) and the pKa of GA was close to 3.6 (Aberkane et al., 2010) which could explain
195 the changes of charges upon pH. In the studied conditions, when the pH value was distant to
196 the pKa of CN, the positive value of Zeta potential increased, suggesting an increase of the
197 cationic charge onto the polymer. Similar results were observed with GA in ultrapure water but
198 not in acetic acid (data not shown). Normally, GA was supposed to be more charged when pH
199 increased beyond its pKa. Nevertheless, in acetic acid solution it was not the case. This may be
200 explained by an increase of the ionic strength when the pH increased due to the addition of
201 NaOH to obtain the targeted pH; indeed it is known that when the ionic strength increases along
202 with the pH, the net charge of the polymer decreases, as it has been shown on pectin, CN and
203 alginate (Abodinar, Smith, & Morris, 2014).

204 It was chosen to focus on the pH 4.5, 5.0 and 5.5, so the pH would be far enough from
205 the pKa of both polysaccharides. As many authors already reported (Butstraen & Salaün, 2014;
206 Espinosa-Andrews et al., 2013), the data from the biopolymers approximate Zeta potentials led
207 to presume that more GA than CN in the mixtures was necessary in order to reach stoichiometry
208 (in other words, the optimal molar ratio where all CN charges were neutralized by GA charges),
209 at any pH (between four and five times more GA than CN in the literature (Butstraen & Salaün,
210 2014; Espinosa-Andrews et al., 2007, 2010)). The results from **Table 1** suggested that the
211 higher the pH, the fewer GA would be needed to neutralize the CN positive charges ($|ZP$
212 $_{CN}/ZP_{GA}|$ of 2.7 for pH 4.5, 2.1 for pH 5.0 and 2.2 for pH 5.5 at 25 °C). Therefore, it seemed
213 that twice the amount of GA compared to CN would be needed to obtain neutral complexes if
214 all the charges were involved in the interaction, for all experimental conditions. The obtained
215 results have also shown that the temperature had no influence over the Zeta potentials of GA.
216 On the contrary, the CN Zeta potentials decreased with the raise of temperature in acetic acid
217 solutions. A raise in temperature would lead to a compaction of CN, decreasing its steric
218 hindrance during self-assembly so the charges would be less available for the interaction.

219 Since this study aimed to understand what drives complex coacervation between GA and
220 CN, ITC measurements were performed in order to elucidate the thermodynamic pathway
221 related to the complexation between GA and CN. Complex coacervation of GA and CN upon
222 molar ratio was thus first investigated.

223 **3.2. Thermodynamic parameters and energies involved in the** 224 **coacervation process**

225 The thermodynamic parameters involved in complex coacervation between GA and CN
226 were determined using ITC (Aberkane et al., 2010; Xiong et al., 2016) at different pH and

227 different temperatures (**Figure 1**). This method leads to determine the stoichiometry (n) of the
228 interaction, if the coacervation is enthalpy-driven or entropy-driven and the related
229 thermodynamic values as ΔG , ΔH , $T\Delta S$ and dissociation constant K_d .

230 Since corrected heat rates were negative in all cases, the interaction major contribution was
231 mostly exothermic (**Figure 1.A and B**) related to a spontaneous phenomenon. The peak areas
232 corresponded to the energy released or absorbed by the cell containing the CN solution after
233 each GA solution injection. A sequence of successive exothermic peaks of decreasing intensity
234 was initially observed in most cases. The binding energy decreased upon GA addition until it
235 stabilized (around the 20th injection). At the end of the experiment, a stabilized sequence of
236 weaker exothermic peaks was always observed, related to a dilution phenomenon. This heat of
237 dilution was nevertheless temperature-dependent (at pH 5.0, -0.2, -0.3 and -0.5 $\mu\text{J}\cdot\text{s}^{-1}$ at 5 °C,
238 25 °C and 45 °C, respectively) and pH-dependent (at 45 °C, -0.3, -0.5 and -0.75 $\mu\text{J}\cdot\text{s}^{-1}$ for pH
239 pH 4.5, 5.0 and 5.5, respectively). Moreover, constant endothermic peaks were observed at the
240 end of titration, when GA was in excess. Peaks intensities varied upon studied conditions, which
241 were more important at 45 °C (between 0.1 to 0.2 $\mu\text{J}\cdot\text{s}^{-1}$) than at 5 °C (0.005 to 0.008 $\mu\text{J}\cdot\text{s}^{-1}$). A
242 switch from an exothermic phenomenon to an endothermic one indicated two successive
243 molecular events (Aberkane et al., 2010; Kayitmazer, 2017). The first one might be attributed
244 to the electrostatic interaction between macromolecules (formation of soluble complexes or
245 coacervates) while the second one could be attributed to aggregation, coalescence of the
246 complexes or to a reorganization of the complexes. In some cases, as for pH 5.0 at 45 °C, at the
247 beginning of titration an increase of the binding energy were observed before titration, which
248 is often encountered in ITC measurements for the first 20 μL injected. It could be explained
249 either by a diffusion of GA into the cell during the temperature equilibration or because the two
250 polymers were forming complexes prior to coacervation, opening the chitosan structure in some
251 conditions. Both pH and temperature influenced the intensity of the exothermic signals of the

252 interaction. At a given pH (**Figure 1.A**), the intensity of the signal increased upon temperature.
253 The same behavior has been observed upon pH at a given temperature (**Figure 1.B**). This was
254 observed at all studied conditions (data not shown).

255 The binding isotherms were then fitted using the “Independent” model in order to obtain
256 the corresponding thermodynamic parameters (**Figure 1.C and D**). At 5 °C, due to weak
257 signals, the repeatability was not optimal. The first five enthalpy values were not taken into
258 account while modeling the raw data (grey dots **Figure 1.C and D**). According to raw data,
259 enthalpy values were increasing in absolute value when the temperature and the pH increased,
260 corresponding to more electrostatic interactions.

261 The enthalpy upon molar ratio followed a typical titration curve with the center of the
262 linear segment of the sigmoid corresponding to the stoichiometry of the interaction (the molar
263 ratio where all the charges of the CN were neutralized by the charges of the GA). Since the
264 inflection point was not always at the same molar ratio, the stoichiometry appeared to be slightly
265 different upon studied conditions. The thermodynamic parameters obtained from the fit and
266 from Eq. 1 and Eq. 2 were given in **Table 2** and are represented on **Figure 2**.

267 For all experimental conditions, ΔG was negative and close to -40 kJ.mol^{-1} which
268 confirmed that the interactions between GA and CN were always spontaneous. ΔH ,
269 corresponding to electrostatic interactions (Aberkane et al., 2010; Duhoranimana et al., 2018;
270 Kayitmazer, 2017; Priftis et al., 2012), was always negative (from -37.6 ± 11.6 to -854.1 ± 45.7
271 kJ.mol^{-1}), so favorable to the interaction (negative contribution to ΔG). $T\Delta S$ was almost always
272 negative, so unfavorable to the interaction (positive contribution to ΔG). The K_d values were
273 always very small (from 1.7×10^{-8} to 26.8×10^{-8}) which meant that the interactions between the
274 two polymers were quite strong because complexes are considered to have high-affinity when
275 their K_d value is smaller than 10^{-6} (Qin & Gronenborn, 2014).

276 The entropic and enthalpic contributions were strongly influenced by temperature and
277 pH. When temperature increased, the entropy significantly ($p\text{-value} = 2.5 \times 10^{-5}$) decreased
278 (from $+0.6 \pm 14.2 \text{ kJ}\cdot\text{mol}^{-1}$ at $5 \text{ }^\circ\text{C}$ to $-519.8 \pm 2.0 \text{ kJ}\cdot\text{mol}^{-1}$ at $45 \text{ }^\circ\text{C}$, at pH 5.0) and the enthalpy
279 significantly ($p\text{-value} = 3.4 \times 10^{-5}$) increased (from $-37.6 \pm 11.6 \text{ kJ}\cdot\text{mol}^{-1}$ at $5 \text{ }^\circ\text{C}$ to -561.6 ± 2.5
280 $\text{kJ}\cdot\text{mol}^{-1}$ at $45 \text{ }^\circ\text{C}$, at pH 5.0). The same phenomenon was observed when pH increased (entropy
281 decreased significantly from $-23.3 \pm 2.3 \text{ kJ}\cdot\text{mol}^{-1}$ at pH 4.5 to $-283.0 \pm 11.8 \text{ kJ}\cdot\text{mol}^{-1}$ at pH 5.5
282 at $25 \text{ }^\circ\text{C}$ with a $p\text{-value}$ of 0.0001, and enthalpy decreased from $-67.7 \pm 2.7 \text{ kJ}\cdot\text{mol}^{-1}$ at pH 4.5
283 to $-322.3 \pm 10.8 \text{ kJ}\cdot\text{mol}^{-1}$ at pH 5.5, at $25 \text{ }^\circ\text{C}$ with a $p\text{-value}$ of 0.0009). The enthalpy became
284 thus more favorable to the interaction when pH and temperature increased, whereas the entropy
285 did not. Enthalpy depended on pH for most systems because it was related to the ionization of
286 the polymers (Feng, Leduc, & Pelton, 2008; Kayitmazer, 2017). Authors have reported that
287 complex coacervation between weak polyelectrolytes was mostly driven by a negative enthalpy
288 due to the electrostatic interactions between two oppositely charged components. However, it
289 was unexpected that the raise in temperature would decrease the entropic contribution to the
290 interaction (Li, Kelkar, & Wagner, 2012; Priftis et al., 2012). This result was unexpected
291 because the opposite is generally observed in the literature (Aberkane et al., 2010; Li et al.,
292 2012; Priftis et al., 2012). Indeed, hydrophobic interactions are enhanced by increasing the
293 temperature due to conformational changes of polysaccharide structure and release of binding
294 water and counterions in the bulk favoring entropic contribution (Kelly, Gudo, Mitchell, &
295 Harding, 1994; Schmitt et al., 1998). In the cases of biopolymer-based complexes, the
296 temperature-induced conformational changes play dominant roles (Dickinson et al., 2001;
297 Priftis et al., 2012; Schmitt et al., 1998). It has also been described that CN hydrodynamic
298 diameter should decrease upon temperature and pH (Chen & Tsaih, 1998; Fan et al., 2012).
299 Furthermore, the CN was degassed and incubated at the temperature of experiment for 20

300 minutes before ITC measurements. At 45 °C, the structure of CN was more compact and
301 binding water was already released before titration. Due to the thermodynamic equilibrium of
302 the sample, the corresponding entropic contribution was not measured. At 45 °C or at pH 5.5,
303 fewer charges onto CN would be available for the GA charges, making the whole system less
304 random, disfavoring entropic contribution. The counterions release entropy only played a minor
305 role, which might be explained by the fact that the two polymers were dialyzed. The unfavorable
306 entropic effects could be due to the loss of polymer conformation freedom after complexation
307 (Dickinson, 2008). When all charges were involved in the interactions, the system became less
308 random and more ordered, which could explain why the entropy was more unfavorable for
309 higher temperatures. Moreover, a more compacted structure lead to a better interaction between
310 CN and GA, since the steric hindrance of CN decreased.

311 The stoichiometry (n) slightly changed upon temperature or pH. For example, it went
312 from 3.2 ± 0.3 at pH 4.5 to 2.7 ± 0.1 at pH 5.5, at 45 °C (with a p-value of 0.02) and to $4.0 \pm$
313 0.1 at 5 °C to 2.7 ± 0.1 at 45 °C, at pH 5.5, with a p-value of 2.2×10^{-6}). The Zeta potential of
314 CN evolved with temperature contrary to the one of GA. The theoretical values of the Zeta
315 potential of the mixtures suggested that the stoichiometry should decrease a little with the raise
316 from pH 4.5 to 5.5 (**Table 1**). However, as mentioned previously, pH and temperature had a
317 small influence over the stoichiometry consistently with the ZP values. The higher the pH, the
318 lower the stoichiometry; at 25 °C the stoichiometry got from 4.1 ± 0.8 at pH 4.5 to 3.3 ± 0.2 at
319 pH 5.5 (with a p-value of 0.07, so the values were not statistically different but the tendency
320 was strong). The higher the temperature, the lower the stoichiometry; at pH 5.5, the
321 stoichiometry got from 4.0 ± 0.1 at 5 °C to 2.7 ± 0.1 at 45 °C (with a p-value of 2.2×10^{-6}). A
322 raise in temperature also meant that the backbones of the polymers were more flexible and more
323 likely to encounter each other since the solvent should be less viscous (Qiao, Di, Ma, Ma, &
324 Xia, 2010; Roy, Ghosh, & Sarkar, 2010). Even if the tendencies were consistent with the

325 expectations regarding the Zeta potential values of both polymers (**Table 1**), the values were
326 not the same (at 25 °C the stoichiometry was expected to decrease from 2.7 ± 0.2 at pH 4.5 to
327 2.2 ± 0.1 at pH 5.5). Furthermore, though the GA Zeta potential did not evolve upon
328 temperature, the CN Zeta potential decreased upon temperature (Filion et al., 2007), so the ratio
329 of charges between the two polymers became smaller.

330 It can also be noted that the thermodynamic parameters and stoichiometry were really close
331 between pH 4.5 at 25 °C and pH 5.5 at 5 °C (**Table 2**), and between pH 4.5 at 45 °C and pH
332 5.5 at 25 °C (**Table 2**). This suggested that a raise of pH could be tempered by a decrease in
333 temperature (**Table 2 and Figure 2**). The optical micrographs of these conditions were shown
334 in **Figure 3**. Between pH 4.5 at 45 °C and pH 5.5 at 25 °C and between pH 4.5 at 25 °C and pH
335 5.5 at 5 °C, the objects on the micrographs looked almost the same (same number of coacervates
336 and same average diameter of the coacervates for each combinations). Table of analysis of these
337 micrographs are provided in supplementary material.

338 Even if the enthalpy and entropy varied upon pH and temperature, the Gibbs energy was
339 found to be almost constant whatever the physicochemical conditions (around $-40 \text{ kJ}\cdot\text{mol}^{-1}$).
340 This could mean that the formation of the complexes were not driven by the same forces and
341 that the complexes formed did probably not have the same shape. The Zeta potential of the
342 mixtures in the different conditions were measured to appreciate how it coincided with the ITC
343 measurements. The macroscopic aspect of the samples, the turbidity of the mixtures and the
344 shape of the complexes observed from optical microscopy were studied to corroborate ITC data.

345 **3.3. Turbidimetric and Zeta potential measurements and optical**
346 **microscopy upon molar ratio of gum Arabic and chitosan complex**
347 **coacervation**

348 The influence of the GA/CN molar ratio on the coacervate formation was investigated
349 **(Figure 4)**. These experiments were performed at pH 5.0 so the pH would be far enough from
350 the pKa of both polymers, in order for them to be charged. For CN and GA mixtures, Zeta
351 potential and turbidity were measured.

352 When the two polymers solutions were mixed together the sample became turbid, which
353 meant new objects were formed **(Figure 4)**. Moreover, after 24 hours, two different phases
354 appeared (data not shown). The upper phase was transparent, the phase below was turbid: it
355 was a liquid/liquid associative phase separation (complex coacervation). It is known that
356 coacervates are not stable and that they coalesce upon time. Knowing this, it is important to
357 characterize the samples in the same conditions, so all measurements were made 5 minutes after
358 mixing the solutions. The turbidity of the mixture increased from $0.283 \pm 0.088 \text{ cm}^{-1}$ at the ratio
359 1:1 to $2.744 \pm 0.392 \text{ cm}^{-1}$ at the ratio 4:1. Ratio 4:1 to ratio 10:1 were not statistically different
360 from each other ($p_0 > 0.05$). However the turbidity seemed to have a tendency to decrease with
361 the increase of the GA proportion in the mixtures **(Figure 4)**. This decrease can either be related
362 to a change of structure of the objects, or to a dilution of the system. The volumes of GA added
363 excluded the dilution hypothesis. In addition, a change of structure of the complexes would be
364 consistent with the endothermic peaks at the end of ITC titration **(Figure 1.A and B)**.

365 This result was consistent with published data from other authors and with the ITC
366 stoichiometry **(Table 2 and Figure 2)**: at 25 °C pH 5.0, the stoichiometry was 4.0 ± 0.9 and in
367 the literature, in the same conditions, optimal molar ratios were in a range from 4 to 5 (Butstraen

368 & Salaün, 2014; Espinosa-Andrews et al., 2007). Objects were formed when the molar ratio
369 was sufficient, in other words when there was enough GA to neutralize the charges of CN.
370 When the molar ratio GA/CN was higher than 4:1 the turbidity decreased. This phenomenon
371 could be explained by a reorganization of the coacervates due to an excess of GA in order to
372 obtain thermodynamic equilibrium in the system. These results were corroborated with optical
373 microscopy discussed farther (**Figure 5**) and with the sequence of endothermic peaks obtained
374 at the end of titration by ITC measurements (**Figure 1**).

375 The Zeta potential of the objects has also been investigated. For molar ratio below 1:1,
376 CN was in excess so the mixture Zeta potential was close to the one of CN (21.6 ± 0.8 mV).
377 When more gum was added, the Zeta potential got closer to neutrality (around ratio 3:1).
378 Finally, when GA was in excess, the Zeta potential of the mixture tended to the one of GA ($-$
379 10.2 ± 0.2 mV, **Table 1**). Similar results with mixtures GA/CN at different pH were already
380 published by Butstraen *et al.*, 2014 and Espinosa-Andrews *et al.*, 2007 (Butstraen & Salaün,
381 2014; Espinosa-Andrews et al., 2007). The maximum turbidity (2.744 ± 0.362 cm⁻¹) was
382 observed when the Zeta potential value was close to zero at a molar ratio of 4:1, which was
383 consistent with the ITC stoichiometry in these given conditions (4.0 ± 0.9) (Coelho et al., 2011).
384 Optical micrographs of the mixtures were collected to study the shape of the objects and to
385 confirm if the loss of turbidity was due to dilution or to a change of shape of the coacervates.
386 In the ITC measurements (**Figure 1**) when the GA was in excess, there was an exothermic/
387 endothermic sequence which would support the theory of complexes reorganization.

388 For molar ratios below 3:1, no object was observed. From ratio 3:1, some coacervates
389 appeared. When more GA was added (from molar ratios 4:1) more coacervates were formed
390 (**Figure 5**), from 88 ± 8 coacervates in the optical field for 3:1 to 747 ± 82 for 4:1. Table of
391 results from image analyses is provided in supplementary material. These molar ratios were

392 consistent with the ITC molar ratio at 25 °C, pH 5.0 (4.0 ± 0.9). For molar ratios above 6:1 (245
393 ± 59 coacervates in the optical field for 6:1), the coacervates size and number decreased and
394 then disappeared (molar ratio 10:1). These results were consistent with the turbidity behavior
395 of the mixtures and their macroscopic aspects (**Figure 4 and Figure 5**). For extreme ratios (1:1
396 and 10:1), due to low turbidity, no object was observed by optical microscopy. It was possible
397 that complexes were formed at these ratios but that they were too small to be observed by optical
398 microscopy. A change of the size and shape of the objects, observed when the molar ratio
399 increased, was consistent with the endothermic sequences observed on the ITC measurements
400 (**Figure 1**). Moreover, a change of the shape of the complexes observed by optical micrographs
401 confirmed the absence of dilution phenomenon.

402 From the microscopy observations, one can note that the polydispersity of size of the
403 objects was quite high. CN had indeed non-charged polar residues (Coelho et al., 2011) because
404 its deacetylation degree was around 75%, so 25% of its N-acetylglucosamine residues were not
405 charged and GA has large non-charged segments. Indeed, GA contains only 23% of glucuronic
406 acid, which are the GA residues charged when deprotonated (Coelho et al., 2011; Renard et al.,
407 2006). The charges were heterogeneously distributed on polydisperse polymers, which can
408 explain the irregularity of the sizes of the coacervates.

409 The optimal molar ratio for the formation of coacervate determined by optical microscopy
410 (between to 4:1 and 5:1) was consistent with the stoichiometry determined from ITC
411 measurements (4.0 ± 0.9 for pH 5.0 at 25 °C) (**Figure 1**) and the optimal ratio obtained by Zeta
412 potential measurements (3.2 ± 0.2), when the value was close to zero and with the maximum
413 turbidity of the mixture (4.0 ± 0.4). However, the first complexes were formed for a ratio 3:1,
414 but other phenomenon occurred for higher molar ratio. On the **Figure 5** from molar ratio 4:1 to
415 5:1 the coacervates were different, which could be explained by a reorganization of the system.

416 The loss in turbidity along with the increase of the ratio could be explained by a reorganization
417 of the complexes to achieve thermodynamic equilibrium. These results were also observed on
418 the optical micrographs and were correlated by the ITC measurements.

419 These interactions between the polymers were indeed partially driven by the pH-related
420 net charge of the two polymers. The influence of the pH on the interactions between GA and
421 CN had thus been investigated.

422 **3.4. Effect of the pH of the solutions on the interactions between gum** 423 **Arabic and chitosan**

424 From ITC results, it seemed that the major interaction that drove complex coacervation
425 was the electrostatic interactions related to the enthalpy (**Table 2** and **Figure 2**). Since the
426 charges of CN varied upon pH (**Table 1**), the influence of pH on the mixtures was investigated.
427 These experiments were conducted at 25 °C. The approximate Zeta potential of the mixtures
428 was measured at pH 4.5, 5.0 and 5.5 for different molar ratios (**Figure 6.A**). For low GA/CN
429 molar ratio (below 1:1), the approximate Zeta potential was close to the one of CN (21.6 ± 0.8
430 mV). The more GA was added, the lower the Zeta potential of the mixture got until it almost
431 reached the GA Zeta potential (-10.2 ± 0.2 mV, **Table 1**). At pH 4.5, 5.0 and 5.5, the Zeta
432 potential reached zero for a molar ratio of 3.0:1; 3.3:1 and 2.4:1, respectively (**Figure 6A**).
433 Turbidity measurements were conducted at low molar ratio (1:1) and at optimal molar ratio for
434 pH 5.0 (4:1) determined by ITC (**Figure 6B**).

435 For the molar ratio 1:1, the turbidity was low all along the pH range (0.089 ± 0.005 and
436 0.164 ± 0.007 cm⁻¹ at pH 4.5 and 5.0, respectively) but it was higher at pH 5.5 (0.293 ± 0.011
437 cm⁻¹) (**Figure 6.B**). From the results obtained by optical micrographs and ITC (**Figure 5** and
438 **Table 2**), the molar ratio 4:1 was supposed to be almost optimal at pH 5.0. At this ratio, when

439 the pH increased, the turbidity decreased from $2.953 \pm 0.044 \text{ cm}^{-1}$ at pH 4.5 to 2.554 ± 0.033
440 cm^{-1} at pH 5.5 (**Figure 6**). Indeed, the higher the pH, the smaller the difference of charge
441 between GA and CN (**Table 1**) and the lower the stoichiometry, as the tendencies have been
442 seen previously in the ITC results ($n = 4.1 \pm 0.8$ at pH 4.5 and $n = 3.3 \pm 0.2$ at pH 5.5) and with
443 the Zeta potential data (the Zeta potential reached zero for a molar ratio of 3.0:1 at pH 4.5 and
444 2.4:1 at pH 5.5). There should be one optimal molar ratio for each pH.

445 From the optical micrographs (**Figure 7**) coacervates were formed for all pH for a ratio
446 of 4:1. At ratio 1:1, no visible coacervate was formed at pH 4.5 and 5.0, whereas some
447 coacervates were formed at pH 5.5. This result was consistent with the Zeta potential and
448 turbidity of the mixtures (**Figure 6**). For a molar ratio of 4:1, though pH had no influence over
449 the size or polydispersity of the coacervates formed, it impacted the number of coacervates (264
450 ± 18 coacervates in the optical field for pH 4.5, 747 ± 82 for pH 5.0 and 353 ± 17 for pH 5.5).
451 Table of results from image analyses is provided in supplementary material.

452 At different pH, the complexes between GA and CN had different shapes and were driven
453 by different enthalpy and entropy contributions. According to ITC results (**Figure 1**) at $25 \text{ }^\circ\text{C}$
454 the stoichiometry at pH 4.5 would be 4.1 ± 0.8 , at pH 5.0: 4.0 ± 0.9 and at pH 5.5: 3.3 ± 0.2 .
455 Ever for low molar ratios, it was possible to obtain coacervates by decreasing pH. ITC
456 measurement also revealed that the interactions were also different upon temperature. At pH
457 5.0, the complex coacervation of GA and CN was then investigated at different temperatures
458 (5, 25 and $45 \text{ }^\circ\text{C}$).

459 **3.5. Effect of the temperature of the solutions on the interactions**
460 **between gum Arabic and chitosan**

461 At the beginning of titration, the Zeta potential (**Figure 8**) corresponded to the one of the
462 CN (21.6 ± 0.8 mV), and at the end of the titration, the Zeta of the mixture corresponded to the
463 one of GA alone (-10.2 ± 0.2 mV). Between the beginning and the end of the titration, for all
464 temperatures the Zeta potential decreased. However, it differed according to the temperature.
465 The stoichiometry decreased when temperature increased (**Figure 8**) as observed by ITC.
466 Indeed the molar ratio for which the approximate Zeta potential was close to 0 mV varied with
467 temperature from 4.2:1 at 5 °C to 3.4:1 at 25 °C and 2.5:1 at 45 °C at pH 5.0 (against $3.8:1 \pm$
468 0.2 , $4.0:1 \pm 0.9$ and $2.9:1 \pm 0.2$ with the ITC, respectively). These results were strongly
469 consistent with the ones obtained from ITC (**Table 2** and **Figure 2**).

470 These results were consistent with the previous hypothesis: this could mean that the CN
471 had different conformation at different temperatures and that some of its charges were not
472 accessible at high temperatures (the stoichiometry being reached for lower molar ratio at 45 °C
473 than at 5 °C). At 5 °C, more GA was needed to counter the charges of the CN because more
474 CN charges were accessible, so the enthalpy was less favorable than at 45 ° (**Table 2** and **Figure**
475 **2**). The aspect of the sample has been investigated by optical microscopy (**Figure 9**).

476 At molar ratio 1:1, whatever the temperature, no object was formed. At molar ratio 4:1,
477 coacervates were observed for all temperatures and the complexes formed were strongly
478 different. However, the number and shape of the coacervates varied upon temperature. At 5 °C,
479 the coacervates were less numerous than at 25 °C (**Figure 9**) (63 ± 9 coacervates in the optical
480 field at 5 °C against 747 ± 82 at 25 °C). Table of results from image analyses is provided in
481 supplementary material. Temperature seemed to have an impact on the size of the coacervates,

482 as reported previously in this study. At 45 °C for a ratio of 4:1, the coacervates were bigger and
483 less numerous (the average diameter of the coacervates was $7.3 \pm 0.8 \mu\text{m}$ at 45 °C against 3.6
484 ± 0.5 at 25 °C and the number of coacervates was 173 ± 36 at 45 °C), which could be explained
485 by a coalescence phenomenon of the complexes at higher temperature. Even though the
486 coacervates were bigger, no settling was observed 5 minutes after mixing.

487 **3.6. Possible mechanism of the interaction between gum Arabic and** 488 **chitosan**

489 From previous experiments, it was observed that pH, temperature and molar ratio strongly
490 influenced the coacervation phenomenon, in terms of thermodynamic pathway and structural
491 aspects of the objects formed. The obtained results allowed us to propose a mechanism involved
492 in the formation of GA/CN complexes (**Figure 10**).

493 The complex coacervation between GA and CN were investigated. When mixed in
494 solution, those two oppositely charged polysaccharides formed a turbid dispersion which led to
495 assume they were forming complexes (**Figure 4**). The optical micrographs of the mixtures in
496 different conditions of pH and temperature showed that these parameters had a significant
497 influence over the complexes formed (**Figure 10**). The different thermodynamic parameters
498 obtained for each condition confirmed this influence (**Table 2** and **Figure 2**).

499 In order to study the influence of the molar ratio, the interactions between GA and CN
500 were investigated at a given pH and a given temperature. At a ratio of 1:1, no complexe was
501 visible (pH 5.0, 25 °C, **Figure 10.A**). However, it was possible that objects were formed (GA
502 charges would interact with CN charges), but that they were too small to be seen by optical
503 microscopy. When more GA was added to the CN, more charges of the polymers interacted.
504 The stoichiometry value determined by ITC was confirmed from optical microscopy (ratio 4:1),

505 turbidity (maximum turbidity between ratios 3:1 to 4:1) and Zeta potential (close to 0 between
506 3:1 and 4:1). Upon molar ratio, visible complexes were indeed formed (ratio 3:1) and all GA
507 charges interacted with all CN charges, obtaining neutral visible coacervates. At a ratio 6:1,
508 when GA was in excess, the complexes got smaller. In order to reach an equilibrium in the
509 system, the GA could desorb and the coacervates could change. This hypothesis is consistent
510 with the small endothermic event at the end of titration (ITC results, **Figure 1**). This could be
511 explained by this reorganization within the system.

512 To study the influence of the pH, the interactions between GA and CN were investigated
513 at a given temperature and a given molar ratio (25 °C, ratio 1:1, **Figure 10.B**). The complexes
514 were different upon pH. At pH 4.5 and 5.0, no complex was observed. At pH 5.5, visible
515 coacervates were formed. Even at a small molar ratio, it was possible to have a coacervation
516 phenomenon by tempering with the pH, since pH affected the Zeta potential of CN (**Table 1**),
517 so less GA would be needed to achieve stoichiometry. The optimal molar ratio was smaller at
518 higher pH ($2.2:1 \pm 0.1$ at pH 5.5 against $2.7:1 \pm 0.2$ at pH 4.5). Since when the pH raised, the
519 Zeta potential of CN decreased, there were fewer free charges available for the interaction in
520 the system which might explain that the entropy was less favorable when the pH increased (the
521 system was more ordered).

522 To study the influence of the temperature, the interactions between GA and CN were
523 investigated at a given pH and a given molar ratio (pH 5.0, ratio 4:1, **Figure 10.C**). The
524 complexes between GA and CN changed upon temperature in the same way that they did upon
525 pH. When GA was in excess (more GA than was necessary to achieve stoichiometry), at 25 °C,
526 more coacervates were formed. At 45 °C, the coacervates were bigger, suggesting a coalescence
527 of the coacervate because of enhanced thermal motion at this temperature. At a given pH, there
528 was an optimal molar ratio for each temperature (**Figure 10.C**). This was inherent to the shape

529 of the polymers at different temperature, especially the one of CN. Indeed, CN was compacted
530 at 45 °C, so less charges were available for the interaction, needing less GA to achieve
531 stoichiometry. This was consistent with the stoichiometry determined by ITC. The fewer GA
532 involved in the interaction, the smaller the coacervates.

533 For each pH-temperature combination, there was an optimal molar ratio for coacervation.
534 For example, at a pH 5.0, at 5 °C the optimal molar ratio was 4:1, and at 25 and 45 °C the
535 stoichiometry was around 3:1 and 2:1, respectively (**Figure 10**). The size and shape of the
536 coacervates changed upon pH, temperature and molar ratio.

537 **4. Conclusions**

538 The interactions of gum Arabic (GA) and chitosan (CN) in solution have been
539 investigated upon pH (4.5, 5.0 and 5.5) and temperature (5, 25 and 45 °C). The stoichiometry
540 and the thermodynamic parameters of the interaction in these conditions were determined using
541 ITC. The approximate Zeta potential and the turbidity were confirmed to be strong methods to
542 approximate the stoichiometry of the interaction. For each pH-temperature combination, there
543 was a given optimal molar ratio. The interaction was always spontaneous (ΔG negative) and it
544 was always enthalpy-driven (negative enthalpy). Unlike what can be found in literature, a raise
545 in temperature also favored electrostatic interactions between GA and CN, which was related
546 to the conformation and charges of the polymers. A raise in temperature lead to a compaction
547 of CN and to a diminution of its steric hindrance and to the accessibility of its charges, forming
548 coacervates for lower molar ratios. The same phenomenon happened upon a raise of pH. High
549 temperatures favored coalescence leading to a more ordered system, disfavoring entropy
550 (negative entropy parameter). It was also shown that a raise of pH could be tempered by a
551 decrease in temperature in order to obtain the same objects, using a close thermodynamic

552 pathway. Even for low molar ratios, by choosing a fitted pH/temperature combination, it was
553 possible to form coacervates. Based on these results, it should be possible to control the
554 formation of complexes by controlling the pH-temperature combination.

555 In the different conditions studied, different shaped-complexes were formed. The way
556 they were formed and the shape of the objects might strongly influence their capacity to
557 encapsulate and to deliver a molecule of interest. This study showed that by knowing the
558 charges of polymers upon different parameters, it could be possible to predict the effect of these
559 parameters on the coacervation of these polymers. It would also be interesting to find the better
560 pH/temperature combination to limit coalescence. Moreover, it would be interesting to study
561 the influence of ionic strength on the coacervates formation, due to the presence of counterions
562 masking the charges. Now that the mechanism and driving forces of the interactions are better
563 understood, it should be used to investigate the relation between the shape of the complexes
564 and their ability to encapsulate a molecule and to study the impact of the molecule on the
565 coacervate added during the coacervates formation. Hopefully the different forms of the
566 complexes could lead to encapsulation in different medium and to deliver the molecule to a
567 chosen target. Other shapes of complexes could be obtained by taking other polymers or by
568 modifying GA or CN for example.

569 **Acknowledgments**

570 The authors acknowledge support of the LIBio by the "Impact Biomolecules" project of
571 the "Lorraine Université d'Excellence"(Investissements d'avenir – ANR).

572 The authors acknowledge support of the CPER Agrovalor.

573 We would like to thank Nexira for kindly providing the **gum** Arabic used in this article.

574 We also thank Aurélie Seiler and Blandine Simard for the technical support.

575 **References**

576 Aberkane, L., Jasniewski, J., Gaiani, C., Scher, J., & Sanchez, C. (2010). Thermodynamic
577 characterization of acacia gum-beta-lactoglobulin complex coacervation. *Langmuir: The ACS*
578 *Journal of Surfaces and Colloids*, 26(15), 12523–12533. <https://doi.org/10.1021/la100705d>

579 Abodinar, A., Smith, A. M., & Morris, G. A. (2014). A novel method to estimate the stiffness
580 of carbohydrate polyelectrolyte polymers based on the ionic strength dependence of zeta
581 potential. *Carbohydrate Polymers*, 112, 6–9. <https://doi.org/10.1016/j.carbpol.2014.05.063>

582 Anwunobi, A. P., Emeje, M. O. (2011). Recent applications of natural polymers in nanodrug
583 delivery. *Journal of Nanomedicine & Nanotechnology*, s4(1). [https://doi.org/10.4172/2157-](https://doi.org/10.4172/2157-7439.S4-002)
584 [7439.S4-002](https://doi.org/10.4172/2157-7439.S4-002)

585 Avadi, M. R., Sadeghi, A. M. M., Mohammadpour, N., Abedin, S., Atyabi, F., Dinarvand, R.,
586 & Rafiee-Tehrani, M. (2010a). Preparation and characterization of insulin nanoparticles using
587 chitosan and Arabic gum with ionic gelation method. *Nanomedicine: Nanotechnology, Biology*
588 *and Medicine*, 6(1), 58–63. <https://doi.org/10.1016/j.nano.2009.04.007>

589 Beppu, M. M., & Santana, C. C. (2002). Influence of calcification solution on in vitro chitosan
590 mineralization. *Materials Research*, 5(1), 47–50. [https://doi.org/10.1590/S1516-](https://doi.org/10.1590/S1516-59114392002000100008)
591 [14392002000100008](https://doi.org/10.1590/S1516-59114392002000100008)

592 Bhatia, S. R., Khattak, S. F., & Roberts, S. C. (2005). Polyelectrolytes for cell encapsulation.
593 *Current Opinion in Colloid & Interface Science*, 10(1), 45–51.
594 <https://doi.org/10.1016/j.cocis.2005.05.004>

595 Butstraen, C., & Salaün, F. (2014). Preparation of microcapsules by complex coacervation of
596 gum Arabic and chitosan. *Carbohydrate Polymers*, 99, 608–616.
597 <https://doi.org/10.1016/j.carbpol.2013.09.006>

598 Chen, R. H., & Tsaih, M. L. (1998). Effect of temperature on the intrinsic viscosity and
599 conformation of chitosans in dilute HCl solution. *International Journal of Biological*
600 *Macromolecules*, 23(2), 135–141. [https://doi.org/10.1016/S0141-8130\(98\)00036-1](https://doi.org/10.1016/S0141-8130(98)00036-1)

601 Coelho, S., Moreno-Flores, S., Toca-Herrera, J. L., Coelho, M. A. N., Carmo Pereira, M., &
602 Rocha, S. (2011). Nanostructure of polysaccharide complexes. *Journal of Colloid and Interface*
603 *Science*, 363(2), 450–455. <https://doi.org/10.1016/j.jcis.2011.07.098>

604 de Kruif, C. G., Weinbreck, F., & de Vries, R. (2004). Complex coacervation of proteins and
605 anionic polysaccharides. *Current Opinion in Colloid & Interface Science*, 9(5), 340–349.
606 <https://doi.org/10.1016/j.cocis.2004.09.006>

607 Dickinson, E. (2008). Interfacial structure and stability of food emulsions as affected by protein
608 –polysaccharide interactions. *Soft Matter*, 4(5), 932–942. <https://doi.org/10.1039/B718319D>

609 Dickinson, E., Miller, R., Sanchez, C., Despond, S., Schmitt, C., & Hardy, J. (2001). Effect of
610 heat and shear on β -lactoglobulin-acacia gum complex coacervation. *Food Colloids*, 332–342.
611 <https://doi.org/10.1039/9781847550842-00332>

612 Duhoranimana, E., Yu, J., Mukeshimana, O., Habinshuti, I., Karangwa, E., Xu, X. Muhoza, B.,
613 Xia, S., Zhang, X. (2018). Thermodynamic characterization of Gelatin–Sodium carboxymethyl
614 cellulose complex coacervation encapsulating Conjugated Linoleic Acid (CLA). *Food*
615 *Hydrocolloids*, 80, 149–159. <https://doi.org/10.1016/j.foodhyd.2018.02.011>

616 Eratte, D., Wang, B., Dowling, K., J. Barrow, C., & P. Adhikari, B. (2014). Complex
617 coacervation with whey protein isolate and gum arabic for the microencapsulation of omega-3
618 rich tuna oil. *Food & Function*, 5(11), 2743–2750. <https://doi.org/10.1039/C4FO00296B>

619 Espinosa-Andrews, H., Báez-González, J. G., Cruz-Sosa, F., & Vernon-Carter, E. J. (2007).
620 Gum Arabic–chitosan complex coacervation. *Biomacromolecules*, 8(4), 1313–1318.
621 <https://doi.org/10.1021/bm0611634>

622 Espinosa-Andrews, H., Enríquez-Ramírez, K. E., García-Márquez, E., Ramírez-Santiago, C.,
623 Lobato-Calleros, C., & Vernon-Carter, J. (2013). Interrelationship between the zeta potential
624 and viscoelastic properties in coacervates complexes. *Carbohydrate Polymers*, 95(1), 161–166.
625 <https://doi.org/10.1016/j.carbpol.2013.02.053>

626 Espinosa-Andrews, H., Sandoval-Castilla, O., Vázquez-Torres, H., Vernon-Carter, E. J., &
627 Lobato-Calleros, C. (2010). Determination of the gum Arabic–chitosan interactions by Fourier
628 Transform Infrared Spectroscopy and characterization of the microstructure and rheological
629 features of their coacervates. *Carbohydrate Polymers*, 79(3), 541–546.
630 <https://doi.org/10.1016/j.carbpol.2009.08.040>

631 Fan, W., Yan, W., Xu, Z., & Ni, H. (2012). Formation mechanism of monodisperse, low
632 molecular weight chitosan nanoparticles by ionic gelation technique. *Colloids and Surfaces B:*
633 *Biointerfaces*, 90, 21–27. <https://doi.org/10.1016/j.colsurfb.2011.09.042>

634 Fathi, M., Martín, Á., & McClements, D. J. (2014). Nanoencapsulation of food ingredients
635 using carbohydrate based delivery systems. *Trends in Food Science & Technology*, 39(1), 18–
636 39. <https://doi.org/10.1016/j.tifs.2014.06.007>

637 Feng, X., Leduc, M., & Pelton, R. (2008). Polyelectrolyte complex characterization with
638 isothermal titration calorimetry and colloid titration. *Colloids and Surfaces A: Physicochemical*
639 *and Engineering Aspects*, 317(1), 535–542. <https://doi.org/10.1016/j.colsurfa.2007.11.053>

640 Filion, D., Lavertu, M., & D. Buschmann, M. (2007). Ionization and solubility of chitosan
641 solutions related to thermosensitive chitosan/glycerol-phosphate systems. *Biomacromolecules*,
642 8(10), 3224–3234. <https://doi.org/10.1021/bm700520m>

643 Jayme, M. L., Dunstan, D. E., & Gee, M. L. (1999). Zeta potentials of gum arabic stabilised oil
644 in water emulsions. *Food Hydrocolloids*, 13(6), 459–465. [https://doi.org/10.1016/S0268-005X\(99\)00029-6](https://doi.org/10.1016/S0268-005X(99)00029-6)

645

646 Joye, I. J., & McClements, D. J. (2014). Biopolymer-based nanoparticles and microparticles:
647 Fabrication, characterization, and application. *Current Opinion in Colloid & Interface Science*,
648 *19*(5), 417–427. <https://doi.org/10.1016/j.cocis.2014.07.002>

649 Kayitmazer, A. B. (2017). Thermodynamics of complex coacervation. *Advances in Colloid and*
650 *Interface Science*, *239*, 169–177. <https://doi.org/10.1016/j.cis.2016.07.006>

651 Kelly, R., Gudo, E. S., Mitchell, J. R., & Harding, S. E. (1994). Some observations on the nature
652 of heated mixtures of bovine serum albumin with an alginate and a pectin. *Carbohydrate*
653 *Polymers*, *23*(2), 115–120. [https://doi.org/10.1016/0144-8617\(94\)90035-3](https://doi.org/10.1016/0144-8617(94)90035-3)

654 Kim, H. J., Yang, B., Park, T. Y., Lim, S., & Cha, H. J. (2017). Complex coacervates based on
655 recombinant mussel adhesive proteins: their characterization and applications. *Soft Matter*,
656 *13*(42), 7704–7716. <https://doi.org/10.1039/C7SM01735A>

657 Kizilay, E., Kayitmazer, A. B., & Dubin, P. L. (2011). Complexation and coacervation of
658 polyelectrolytes with oppositely charged colloids. *Advances in Colloid and Interface Science*,
659 *167*(1–2), 24–37. <https://doi.org/10.1016/j.cis.2011.06.006>

660 Lankalapalli, S., & Kolapalli, V. R. M. (2009). Polyelectrolyte complexes: a review of their
661 applicability in drug delivery technology. *Indian Journal of Pharmaceutical Sciences*, *71*(5),
662 481–487. <https://doi.org/10.4103/0250-474X.58165>

663 Li, D., Kelkar, M. S., & Wagner, N. J. (2012). Phase behavior and molecular thermodynamics
664 of coacervation in oppositely charged polyelectrolyte/surfactant systems: a cationic polymer JR
665 400 and anionic surfactant SDS mixture. *Langmuir*, *28*(28), 10348–10362.
666 <https://doi.org/10.1021/la301475s>

667 Lopez-Torrez, L., Costalat, M., Williams, P., Doco, T., & Sanchez, C. (2015). Acacia senegal
668 vs. Acacia seyal gums – Part 1: Composition and structure of hyperbranched plant exudates.
669 *Food Hydrocolloids*, *51*, 41–53. <https://doi.org/10.1016/j.foodhyd.2015.04.019>

670 Maqbool, M., Ali, A., & Alderson, P. G. (2010). A combination of gum arabic and chitosan can
671 control anthracnose caused by *Colletotrichum musae* and enhance the shelf-life of banana fruit.
672 *Journal of Horticultural Science & Biotechnology*, *85*(5), 432–436.
673 <https://doi.org/https://doi.org/10.1080/14620316.2010.11512693>

674 Moschakis, T., Murray, B. S., & Biliaderis, C. G. (2010). Modifications in stability and
675 structure of whey protein-coated o/w emulsions by interacting chitosan and gum arabic mixed
676 dispersions. *Food Hydrocolloids*, *24*(1), 8–17. <https://doi.org/10.1016/j.foodhyd.2009.07.001>

677 Overbeek, J. T. G., & Voorn, M. J. (1957). Phase separation in polyelectrolyte solutions. Theory
678 of complex coacervation. *Journal of Cellular and Comparative Physiology*, *49*(S1), 7–26.
679 <https://doi.org/10.1002/jcp.1030490404>

680 Priftis, D., Laugel, N., & Tirrell, M. (2012). Thermodynamic characterization of polypeptide
681 complex coacervation. *Langmuir*, *28*(45), 15947–15957. <https://doi.org/10.1021/la302729r>

- 682 Qiao, Y., Di, Z., Ma, Y., Ma, P., & Xia, S. (2010). Viscosities of pure water, acetic acid + water,
683 and p-Xylene + acetic acid + water at different temperature and pressure. *Chinese Journal of*
684 *Chemical Engineering*, 18(3), 446–454. [https://doi.org/10.1016/S1004-9541\(10\)60242-X](https://doi.org/10.1016/S1004-9541(10)60242-X)
- 685 Qin, J., & Gronenborn, A. M. (2014). Weak protein complexes: challenging to study but
686 essential for life. *The FEBS Journal*, 1948–1949.
687 <https://doi.org/10.1111/febs.12744>
- 688 Renard, D., Garnier, C., Lapp, A., Schmitt, C., & Sanchez, C. (2012). Structure of
689 arabinogalactan-protein from Acacia gum: from porous ellipsoids to supramolecular
690 architectures. *Carbohydrate Polymers*, 90(1), 322–332.
691 <https://doi.org/10.1016/j.carbpol.2012.05.046>
- 692 Renard, D., Lavenant-Gourgeon, L., Ralet, M.-C., & Sanchez, C. (2006). Acacia senegal Gum:
693 continuum of molecular species differing by their protein to sugar ratio, molecular weight, and
694 charges. *Biomacromolecules*, 7(9), 2637–2649. <https://doi.org/10.1021/bm060145j>
- 695 Roldan-Cruz, C., Carmona-Ascencio, J., Vernon-Carter, E. J., & Alvarez-Ramirez, J. (2016).
696 Electrical impedance spectroscopy for monitoring the gum Arabic–chitosan complexation
697 process in bulk solution. *Colloids and Surfaces A: Physicochemical and Engineering Aspects*,
698 495, 125–135. <https://doi.org/10.1016/j.colsurfa.2016.02.004>
- 699 Roy, M. N., Ghosh, G., & Sarkar, L. (2010). Viscous synergic behaviour and solvent–solvent
700 interactions occurring in liquid mixtures of aqueous alkanols with some alkanolic acids. *Physics*
701 *and Chemistry of Liquids*, 48(5), 564–579. <https://doi.org/10.1080/00319100903161507>
- 702 Sakloetsakun, D., Preechagoon, D., Bernkop-Schnürch, A., & Pongjanyakul, T. (2015).
703 Chitosan–gum arabic polyelectrolyte complex films: physicochemical, mechanical and
704 mucoadhesive properties. *Pharmaceutical Development and Technology*, 1–10.
705 <https://doi.org/10.3109/10837450.2015.1035727>
- 706 Sanchez, C., Mekhloufi, G., & Renard, D. (2006). Complex coacervation between β -
707 lactoglobulin and Acacia gum: A nucleation and growth mechanism. *Journal of Colloid and*
708 *Interface Science*, 299(2), 867–873. <https://doi.org/10.1016/j.jcis.2006.02.031>
- 709 Schatz, C., Lucas, J.-M., Viton, C., Domard, A., Pichot, C., & Delair, T. (2004). Formation and
710 properties of positively charged colloids based on polyelectrolyte complexes of biopolymers.
711 *Langmuir*, 20(18), 7766–7778. <https://doi.org/10.1021/la049460m>
- 712 Schmitt, C., Sanchez, C., Desobry-Banon, S., & Hardy, J. (1998). Structure and
713 technofunctional properties of protein-polysaccharide complexes: a review. *Critical Reviews in*
714 *Food Science and Nutrition*, 38(8), 689–753. <https://doi.org/10.1080/10408699891274354>
- 715 Schmitt, C., & Turgeon, S. L. (2011). Protein/polysaccharide complexes and coacervates in
716 food systems. *Advances in Colloid and Interface Science*, 167(1), 63–70.
717 <https://doi.org/10.1016/j.cis.2010.10.001>
- 718 Shaddel, R., Hesari, J., Azadmard-Damirchi, S., Hamishehkar, H., Fathi-Achachlouei, B., &
719 Huang, Q. (2018). Use of gelatin and gum Arabic for encapsulation of black raspberry

- 720 anthocyanins by complex coacervation. *International Journal of Biological Macromolecules*,
721 *107*, 1800–1810. <https://doi.org/10.1016/j.ijbiomac.2017.10.044>
- 722 Soni, B., Mahmoud, B., Chang, S., El-Giar, E. M., & Hassan, E. B. (2018). Physicochemical,
723 antimicrobial and antioxidant properties of chitosan/TEMPO biocomposite packaging films.
724 *Food Packaging and Shelf Life*, *17*, 73–79. <https://doi.org/10.1016/j.fpsl.2018.06.001>
- 725 Sonia, T. A., & Sharma, C. P. (2012). An overview of natural polymers for oral insulin delivery.
726 *Drug Discovery Today*, *17*(13–14), 784–792. <https://doi.org/10.1016/j.drudis.2012.03.019>
- 727 Tan, C., Xie, J., Zhang, X., Cai, J., & Xia, S. (2016). Polysaccharide-based nanoparticles by
728 chitosan and gum arabic polyelectrolyte complexation as carriers for curcumin. *Food*
729 *Hydrocolloids*, *57*, 236–245. <https://doi.org/10.1016/j.foodhyd.2016.01.021>
- 730 Turgeon, S. L., Schmitt, C., & Sanchez, C. (2007). Protein–polysaccharide complexes and
731 coacervates. *Current Opinion in Colloid & Interface Science*, *12*(4–5), 166–178.
732 <https://doi.org/10.1016/j.cocis.2007.07.007>
- 733 Veis, A. (2011). A review of the early development of the thermodynamics of the complex
734 coacervation phase separation. *Advances in Colloid and Interface Science*, *167*(1–2), 2–11.
735 <https://doi.org/10.1016/j.cis.2011.01.007>
- 736 Veis, A., & Aranyi, C. (1960). Phase separation in polyelectrolyte systems. I. Complex
737 coacervates of gelatin. *The Journal of Physical Chemistry*, *64*(9), 1203–1210.
738 <https://doi.org/10.1021/j100838a022>
- 739 Xiong, W., Ren, C., Jin, W., Tian, J., Wang, Y., Shah, B. R., Li, J., Li, B. (2016). Ovalbumin-
740 chitosan complex coacervation: phase behavior, thermodynamic and rheological properties.
741 *Food Hydrocolloids*, *61*, 895–902. <https://doi.org/10.1016/j.foodhyd.2016.07.018>

Figure captions

Figure 1. (A) Corrected heat rate upon time of mixtures of **gum Arabic** and chitosan at pH 5.0 at 5, 25 and 45 °C (A) and at 45 °C at pH 4.5, 5.0 and 5.5, (B) Enthalpy and fit upon **GA/CN** molar ratio of mixtures of **gum Arabic** and chitosan at pH 5.0 at 5, 25 and 45 °C, (C) and at 45 °C at pH 4.5, 5.0 and 5.5 (D)

Figure 2. Influence of pH and temperature on (A) the optimal molar ratio (n), (B) the enthalpic (ΔH) and (C) and the entropic ($T\cdot\Delta S$) contributions of **gum Arabic** and chitosan interactions.

Figure 3. Optical micrographs of **gum Arabic** and chitosan mixtures (A) at pH 4.5 at 25 °C and pH 5.5 at 5 °C and (B) at pH 4.5 at 45 °C and pH 5.5 at 25 °C at 5°C, 5 min after mixing for a **GA/CN** molar ratio of 4:1

Figure 4. Turbidity (cm^{-1}) and approximate Zeta potential (mV), of **gum Arabic** and chitosan mixtures upon **GA/CN** molar ratio at pH 5.0 and 25 °C, 5 min after mixing

Figure 5. Optical micrographs of **gum Arabic** and chitosan mixtures upon different **GA/CN** molar ratios 5 min after mixing at 25 °C, pH 5.0

Figure 6. (A) Approximate Zeta potential (mV) of the **gum Arabic** and chitosan mixtures upon **GA/CN** molar ratios at different pH, at 25 °C and (B) turbidity (cm^{-1}) of **gum Arabic** and chitosan mixtures for **GA/CN** molar ratios of 1:1 and 4:1 at different pH, 5 min after mixing

Figure 7. Optical micrographs of **gum Arabic** and chitosan mixtures upon pH for **GA/CN** molar ratios 4:1 and 1:1 at 25 °C

Figure 8. Approximate Zeta potential (mV) of the **gum Arabic** and chitosan mixtures upon molar ratio at different temperatures, at pH 5.0

Figure 9. Optical micrographs of **gum Arabic** and chitosan mixtures upon different temperatures for **GA/CN** molar ratios 4:1 and 1:1 at pH 5.0

Figure 10. Optical micrographs and schematic representation of the influence of (A) the molar ratio at pH 5.0, 25 °C, (B) the pH at 25 °C, **GA/CN** molar ratio 1:1 and (C) the temperature at pH 5.0, **GA/CN** molar ratio 4:1 on the coacervation of **gum Arabic** and chitosan

Figure 1

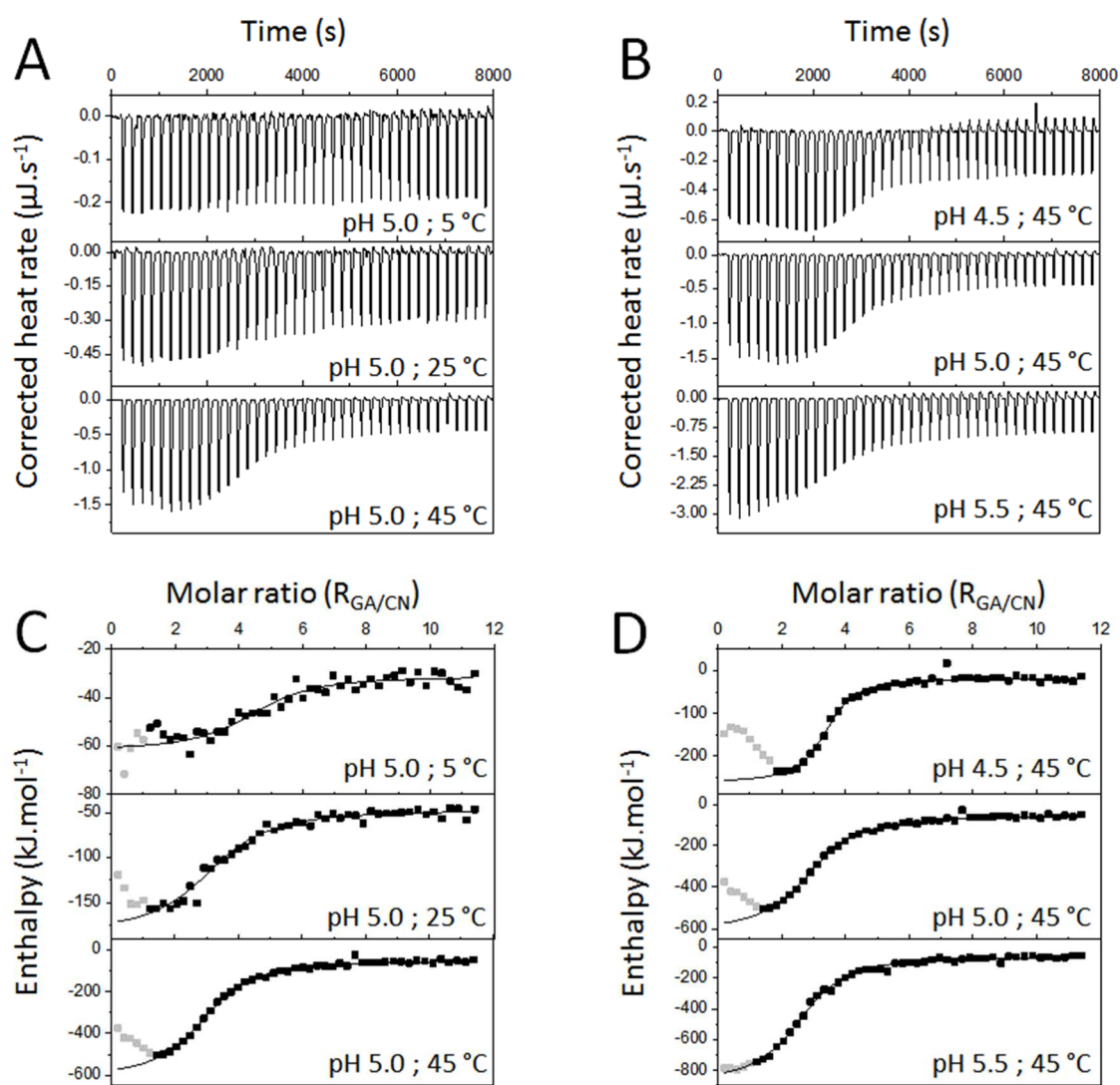


Figure 2

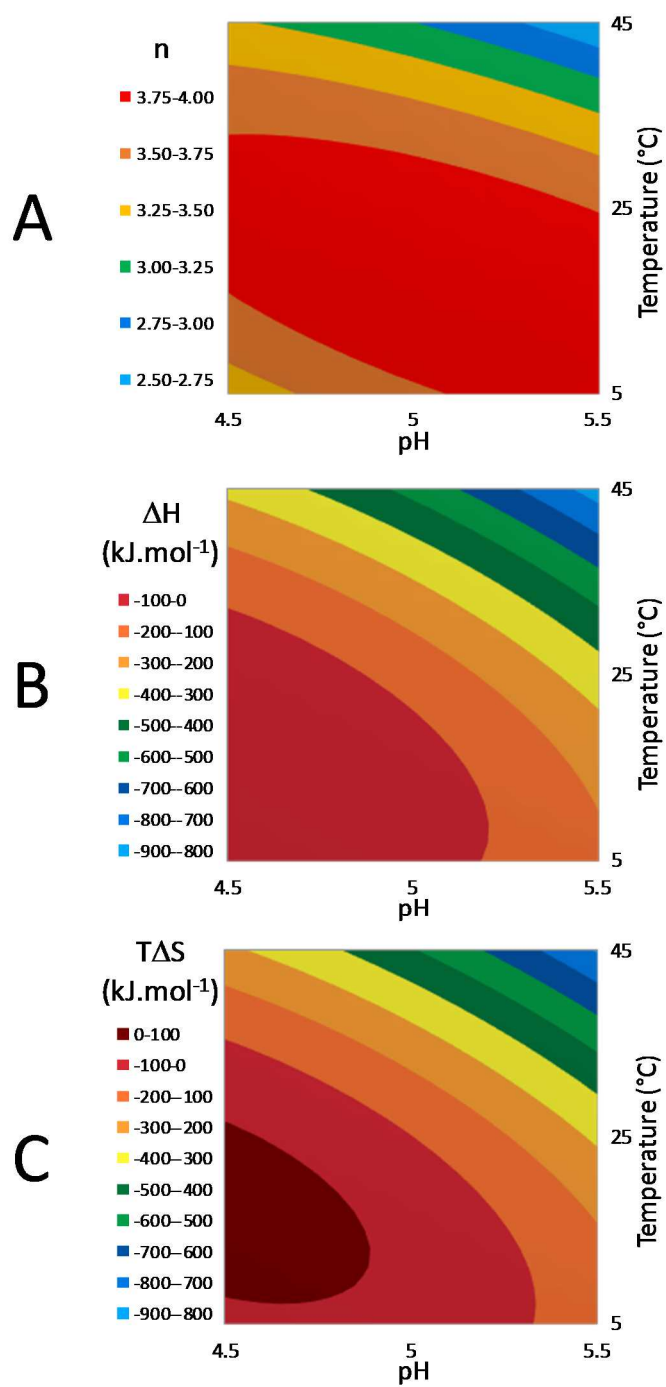


Figure 3

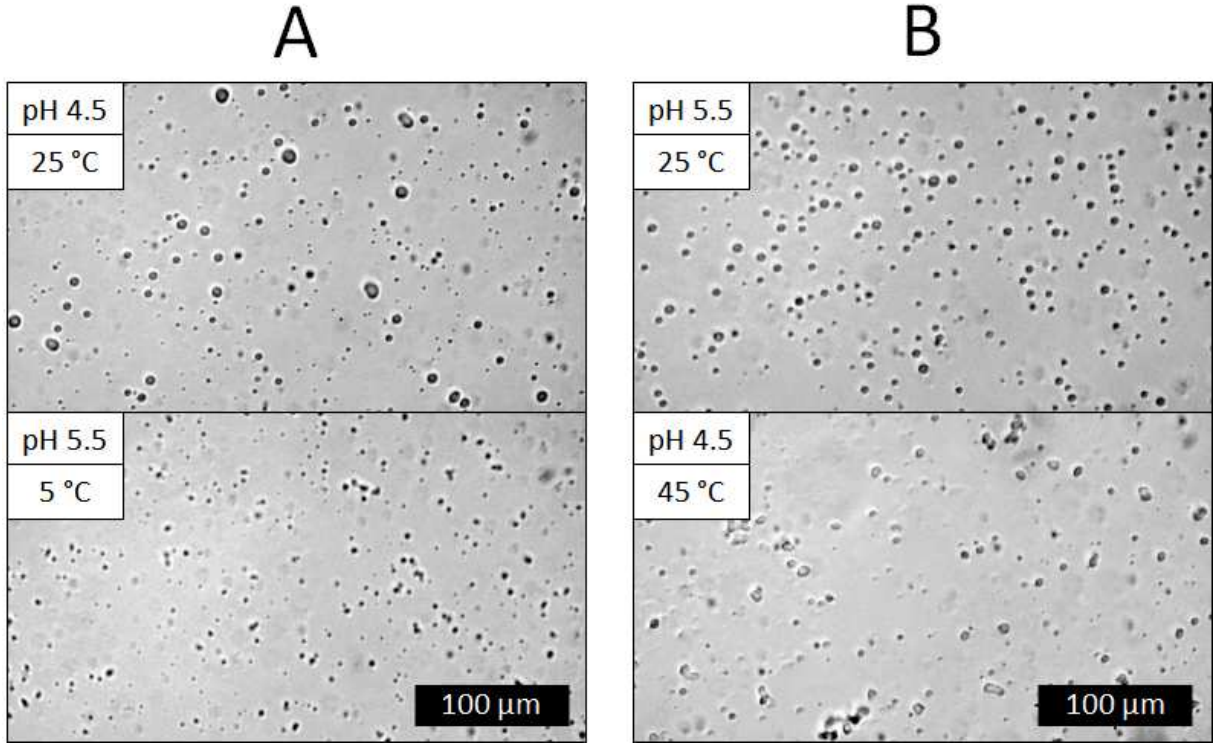


Figure 4

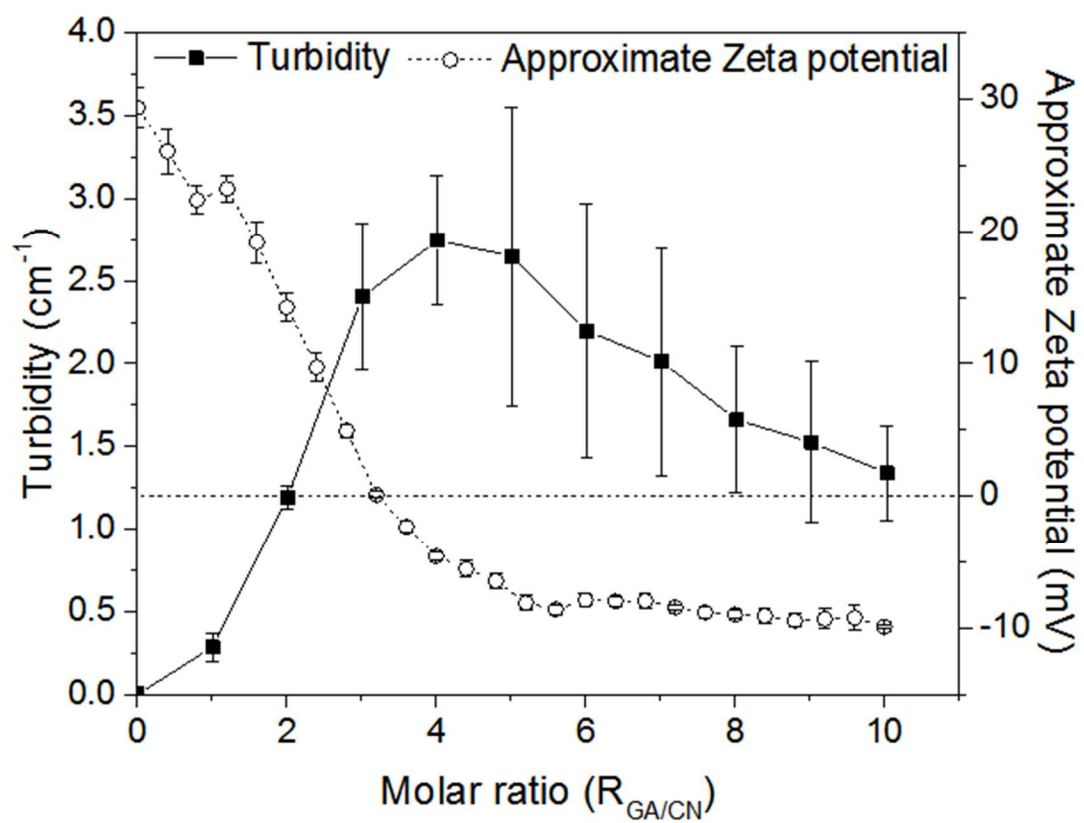


Figure 5

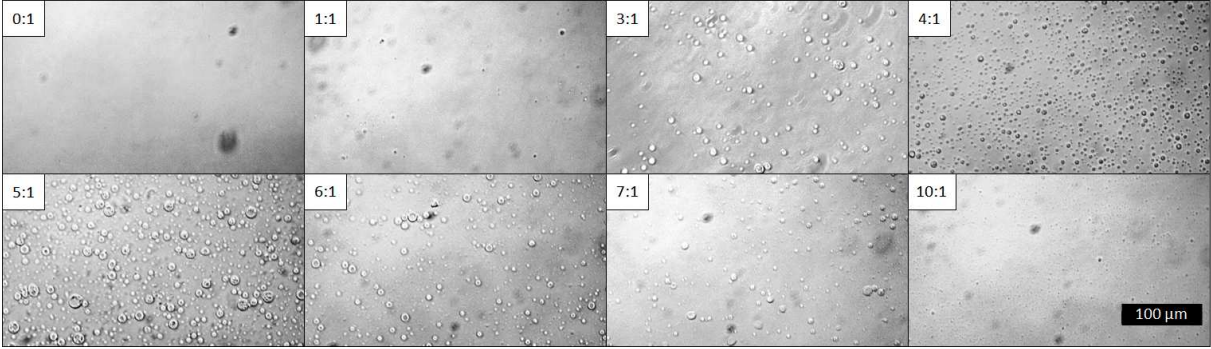


Figure 6

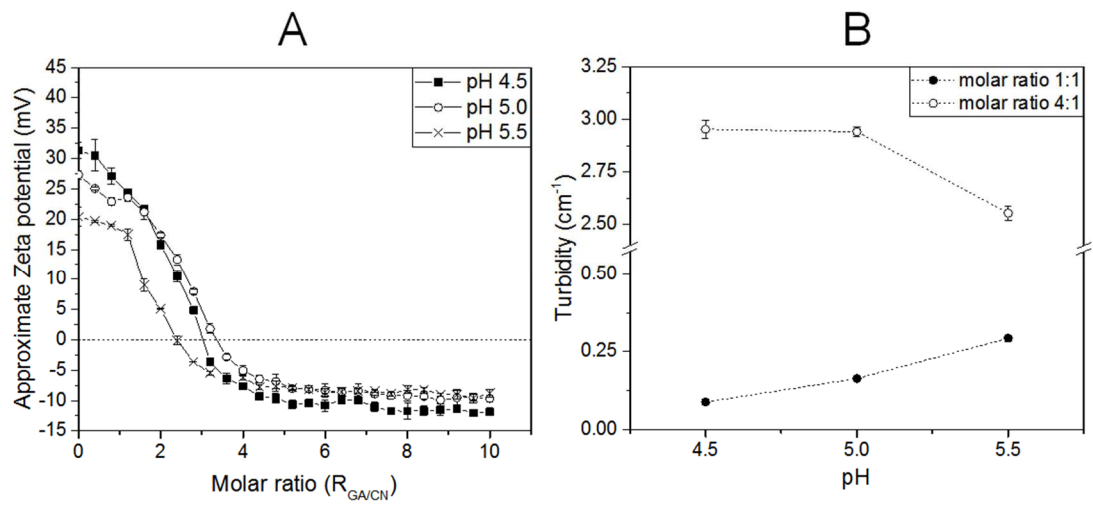


Figure 7

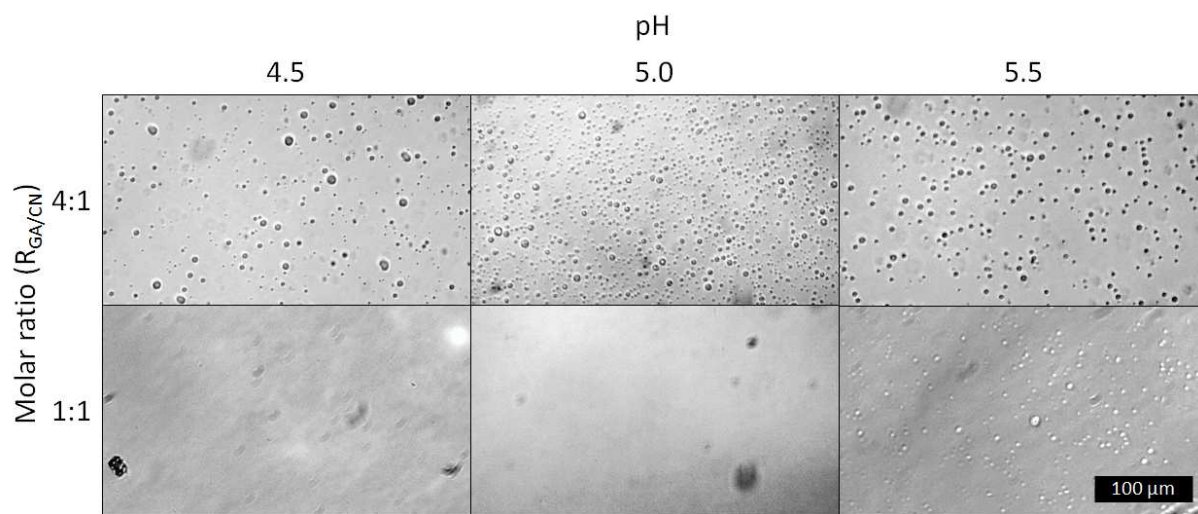


Figure 8

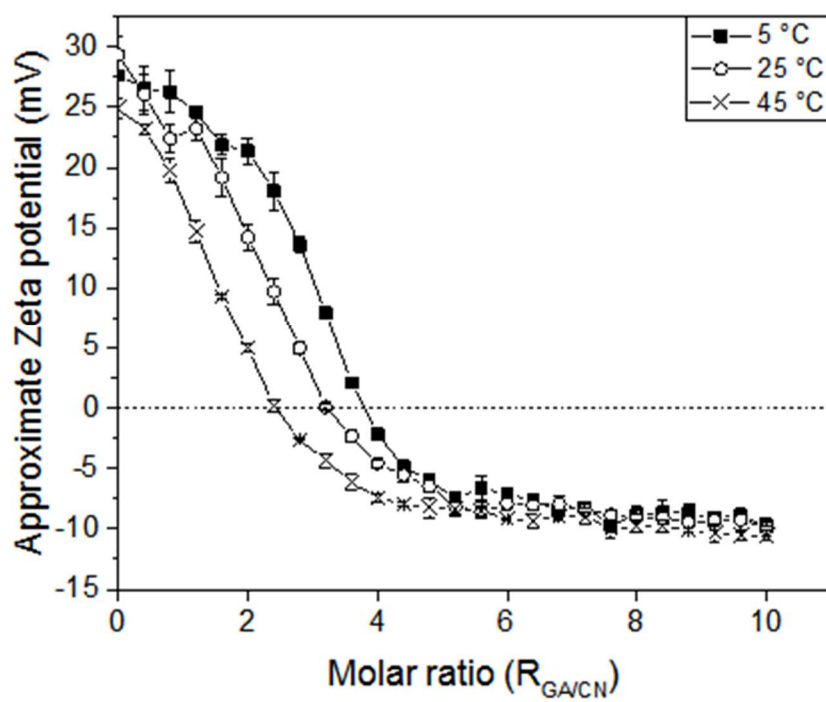


Figure 9

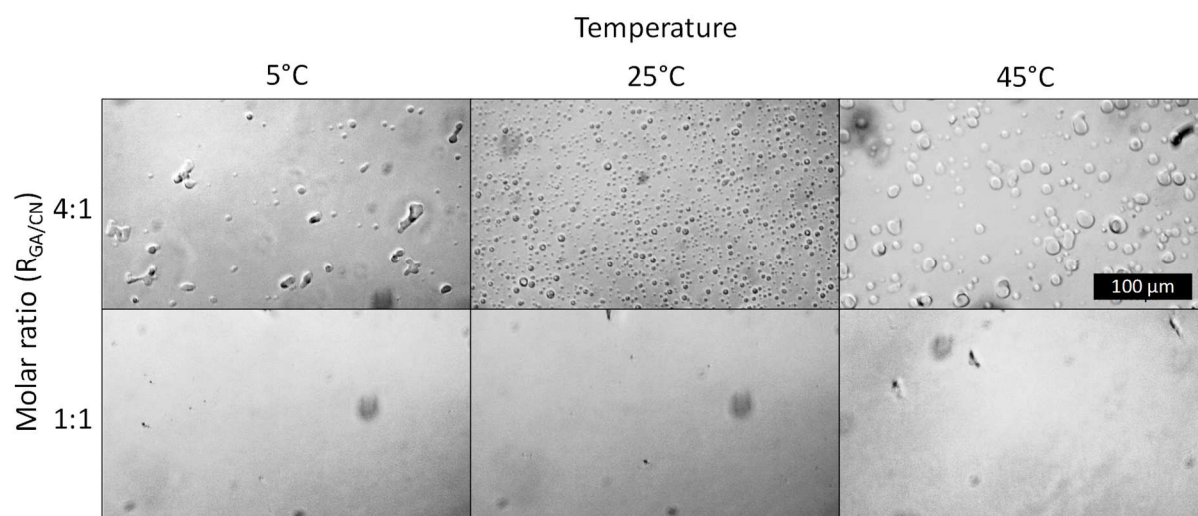


Figure 10

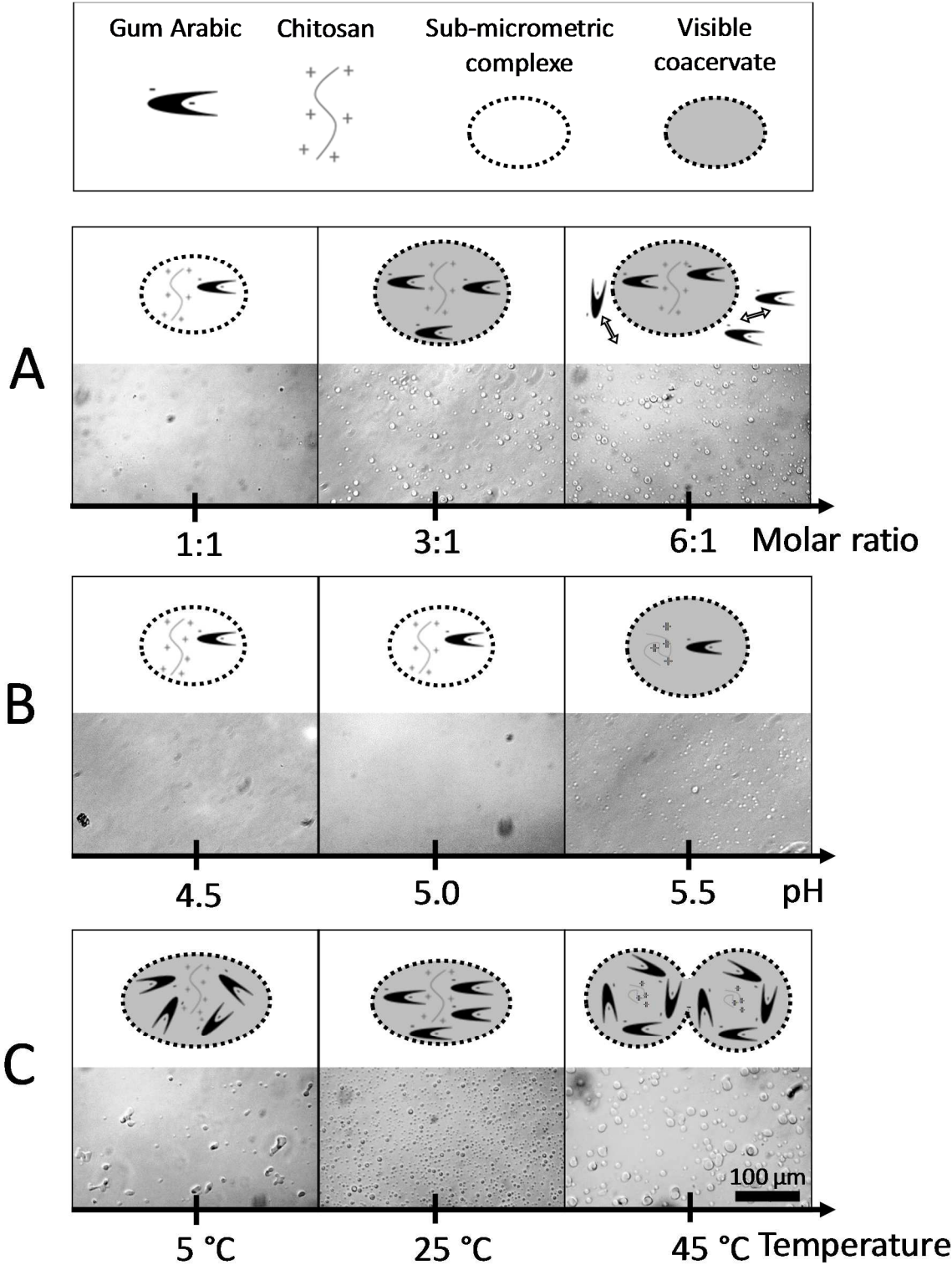


Table captions

Table 1. Approximate Zeta potential of chitosan (0.02% w/v) and **gum Arabic** (1.00% w/v) solutions in acetic acid 1.00% v/v upon pH and temperature and comparative Zeta potential ratios (ZP_{CN}/ZP_{GA}). “a, b, c, d, e and f” mean that the statistical analysis showed no significant differences between the results

Table 2. Thermodynamic parameters (stoichiometry (n), enthalpic contribution (ΔH), entropic contribution ($T\Delta S$), Gibbs free energy (ΔG) and dissociation constant (Kd)) of binding between **gum Arabic** and chitosan upon pH and temperature

Table 1

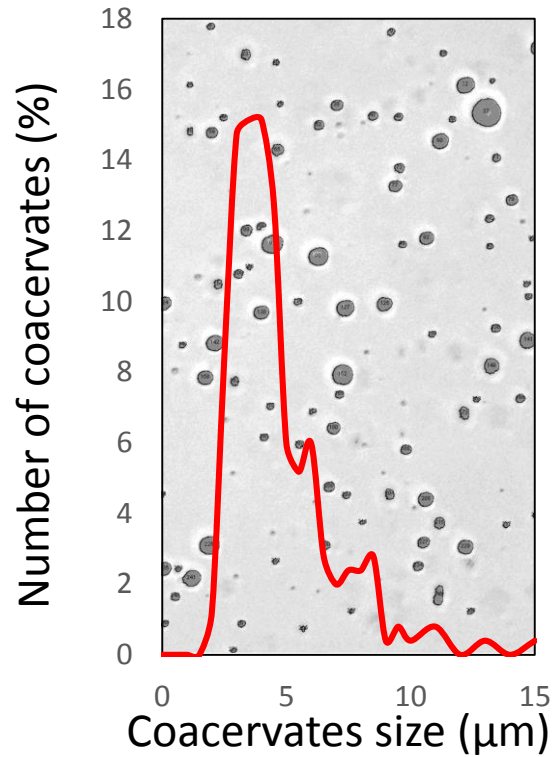
Temperature (°C)	pH	Approximate Zeta Potential (mV)		
		Chitosan 0.02% w/v in acetic acid	Gum Arabic 1.00% w/v in acetic acid	$ ZP_{CN}/ZP_{GA} $
5	4.5	37.2 ± 3.1^a	-9.9 ± 0.4^f	3.1 ± 1.5
	5	22.9 ± 0.7^b	-9.8 ± 1.0^f	2.3 ± 0.2
	5.5	24.5 ± 1.9^b	-9.4 ± 0.2^f	1.6 ± 1.1
25	4.5	28.0 ± 0.9^c	-10.5 ± 0.8^f	2.7 ± 0.2
	5	21.6 ± 0.8^{bd}	-10.2 ± 0.2^f	2.1 ± 0.1
	5.5	20.3 ± 1.0^d	-9.1 ± 0.3^f	2.2 ± 0.1
45	4.5	17.8 ± 0.8^e	-10.3 ± 0.2^f	2.0 ± 0.5
	5	23.0 ± 0.4^b	-9.8 ± 1.2^f	2.2 ± 0.1
	5.5	15.6 ± 1.5^e	-9.1 ± 0.3^f	1.8 ± 0.4

Table 2

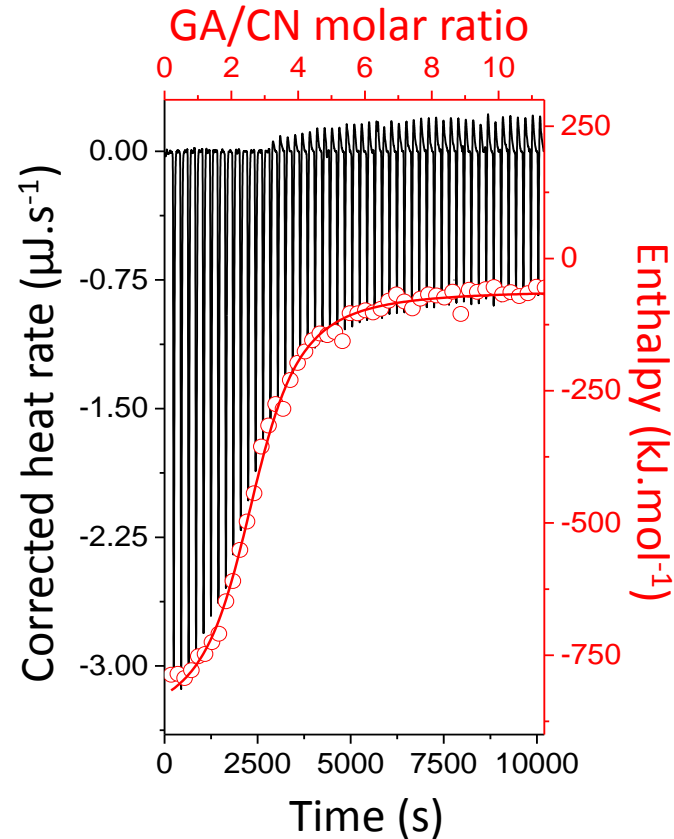
T (°C)	pH	n	ΔH (kJ.mol ⁻¹)	T ΔS (kJ.mol ⁻¹)	ΔG (kJ.mol ⁻¹)	K _d (10 ⁻⁸)
5	4.5	3.0 ± 0.5	-59.6 ± 14.2	-21.3 ± 14.0	-38.3 ± 0.2	6.6 ± 0.7
	5.0	3.8 ± 0.2	-37.6 ± 11.6	+0.6 ± 14.2	-38.2 ± 2.7	13.3 ± 1.8
	5.5	4.0 ± 0.1	-217.1 ± 18.8	-183.3 ± 19.4	-33.8 ± 0.6	26.8 ± 16.9
25	4.5	4.1 ± 0.8	-67.7 ± 2.7	-23.3 ± 2.3	-44.3 ± 0.5	1.7 ± 0.3
	5.0	4.0 ± 0.9	-135.2 ± 0.2	-95.4 ± 2.3	-39.7 ± 2.0	12.9 ± 9.5
	5.5	3.3 ± 0.2	-322.3 ± 10.8	-283.0 ± 11.8	-39.3 ± 0.9	13.5 ± 5.0
45	4.5	3.2 ± 0.3	-293.9 ± 70.6	-249.0 ± 70.7	-44.9 ± 0.1	4.4 ± 0.1
	5.0	2.9 ± 0.2	-561.6 ± 2.5	-519.8 ± 2.0	-41.8 ± 0.5	16.0 ± 2.6
	5.5	2.7 ± 0.1	-854.1 ± 45.7	-812.5 ± 46.0	-41.5 ± 0.3	15.2 ± 1.6

Gum Arabic/Chitosan complex coacervation

Coacervates formation



Isothermal Titration Calorimetry



Temperature favored enthalpy

